Proceedings of the 16th International Heat Transfer Conference, IHTC-16
August 10–15, 2018, Beijing, China

IHTC16-23041

EFFICIENT MODEL FOR EVALUATION OF SPECTRAL AND VERTICAL DISTRIBUTIONS OF ATMOSPHERIC LONGWAVE RADIATION

Carlos F. M. Coimbra,[1,*] Mengying Li,[1] Zhouyi Liao[1]

[1]Department of Mechanical and Aerospace Engineering, Jacobs School of Engineering
Center of Excellence in Renewable Resource Integration and Center for Energy Research
University of California San Diego, 9500 Gilman Drive, La Jolla, CA 92093, USA

ABSTRACT

This work presents an analytical method designed to quantitatively evaluate the spectral and vertical distribution of atmospheric longwave radiation ($0 \sim 2500\,\mathrm{cm}^{-1}$) under clear-sky (cloud-free) conditions. A multilayer plane parallel radiative model with spectral resolution of $0.01\ \mathrm{cm}^{-1}$ is used to model the longwave radiation process in the Earth's atmosphere. An irradiation-radiosity balance for each layer is used to solve for the fluxes for all layers. Broadband contributions of CO_2 to surface downwelling flux and top of atmosphere upwelling flux for different values of water vapor content are found to range from 0.3 to 1.2 $\mathrm{W\,m}^{-2}$ and -0.7 to -0.5 $\mathrm{W\,m}^{-2}$ per 100 ppm increment, respectively. A plating algorithm is adapted for recursive and expedite calculation of modified transfer factors. This modified transfer factors include aerosol reflectance and take into consideration the vertical distribution of spectral thermal fluxes for each layer, including the ground. With the use of modified transfer factors, we found that for an atmosphere with surface relative humidity of 65% and aerosol optical depth at 479.5 nm equal to 0.1, 64.4% of the surface downwelling longwave irradiation is generated from the nearest atmospheric layer, 15.3% from the second nearest layer, 7.5% from the third nearest layer and the remainder 12.8% from other upper layers. From the first atmosphere layer to the tropopause layer, the largest irradiance contribution to each layer is from the layer itself. Above the tropopause, the largest contributor is the ground layer. Layers above the tropopause contribute less than 4.8% to the longwave radiation received by other layers.

KEY WORDS: Spectral radiative model; atmospheric longwave radiation; transfer factors; plating algorithm.

1. INTRODUCTION

Atmospheric longwave radiation (spectral range of 0 to $2500\ \mathrm{cm}^{-1}$) plays a critical role in the thermal budget of the Earth by balancing the shortwave irradiation from the Sun [7]. Small annual variations render downwelling longwave radiation at the Earth's surface a good candidate for monitoring climate change with respect to greenhouse gas build-up [10]. Quantitative evaluation of longwave radiation is also essential in understanding weather and climate variability, as well as to close the thermal balance of solar power plants, cooling towers, buildings and agricultural systems [4, 5, 11, 12]. A spectrally resolved, plane parallel two-flux atmospheric radiative model was previously developed and validated against ground measurements of downwelling longwave radiation [8]. The model was shown to be robust, and to produce results with relative errors of the same order or smaller than the uncertainty of pyrgeometers commonly used for meteorological and climatological applications. Furthermore, the proposed model was able to capture climatic variability between locations when compared to extensive surface telemetry [8]. This work builds on the aforementioned model by adding contributions of the upwelling longwave radiation and analyzing the spectral and vertical contributions of the

*Corresponding Carlos F. M. Coimbra: ccoimbra@ucsd.edu

longwave radiation at all heights of the atmosphere through the use of transfer factors between layers.

2. THE RADIATIVE MODEL

2.1 Model overview

A schematic of the plane parallel model is shown in Fig. 1. The atmosphere is divided into N non-uniform parallel layers according to a pressure ordinates [8]. The standard AFGL midlatitude summer profiles [1] for temperature and atmospheric gas concentrations have been adopted with the correction for current surface atmospheric gas concentrations (in order to allow for different water vapor content and the increasing concentrations of CO_2)[8].The most up-to-date HITRAN data and MT_CKD continuum model are used to calculate spectral and continuum absorption coefficients of gases [3, 9]. The spectral range considered covers from 0 to 2500 cm^{-1} with a resolution of 0.01 cm^{-1}. Mie theory is used to model aerosol absorption and scattering coefficients. The strongly forward scattering of aerosols is re-scaled and approximated by the δ-M approach [6],

$$\hat{\kappa_e} = (1 - \tilde{\rho}_a e_g)\kappa_e; \qquad \hat{\tilde{\rho}} = \frac{\tilde{\rho}(1 - e_g)}{1 - \tilde{\rho}_a e_g}, \tag{1}$$

where the extinction coefficient κ_e and single scattering albedo $\tilde{\rho}$ are scaled using the asymmetry parameter e_g. More details on the comprehensive method and specific submodels can be found in Ref. [8].

2.2 Energy balance between layers

The monochromatic attenuation of intensity along a path s for an isotropic scattering medium is (wavenumber ν is omitted),

$$\frac{dI}{ds} = \kappa_e(1 - \hat{\tilde{\rho}})I_b + \hat{\kappa_e}\hat{\tilde{\rho}}\bar{I} - \hat{\kappa_e}I, \tag{2}$$

where $\hat{\kappa_e}$ (cm^{-1}) is the extinction coefficient (δ-M scaled), $\hat{\tilde{\rho}}$ is the single scattering albedo (δ-M scaled), I_b ($\text{W cm m}^{-2}\,\text{sr}^{-1}$) is the blackbody intensity in wavenumber basis, $I_b(\nu, T) = 2hc^2\nu^3/(\exp\frac{hc}{k_B T\nu} - 1)$, $\bar{I}$ is the

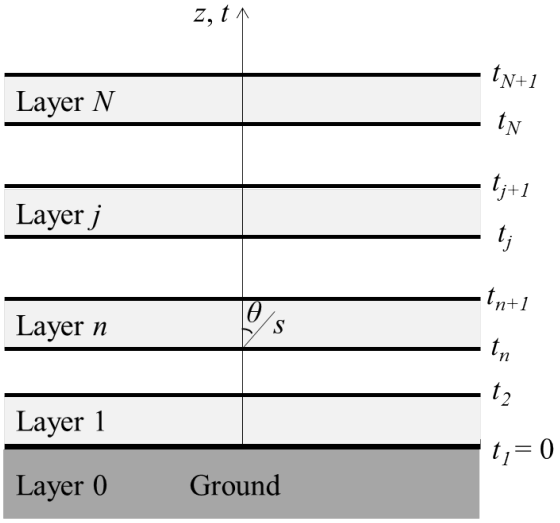

Fig. 1 Schematic of the plane parallel geometry.

averaged intensity over all solid angles, $\bar{I} = 1/4\pi \iint_0^{4\pi} I d^2\omega$. The radiosity J and irradiance G of a volume are,

$$J = (1-\hat{\tilde{\rho}})\pi I_b + \hat{\tilde{\rho}}\pi\bar{I}; \qquad G = \int_0^s e^{-t_{s'}} J(s')ds', \tag{3}$$

where the optical depth $t_{s'} = \int_0^{s'} \hat{\kappa_e}(s'')ds''$.

For a plane parallel layer of atmosphere as shown in Fig.1, the irradiance is expressed using *transfer factors*,

$$G_n = \sum_j J_j \mathcal{F}_{n,j} = \sum_j J_j \frac{1}{4\pi} \iint_0^{4\pi} \left[e^{t_s - t_{s,j}} - e^{t_s - t_{s,j+1}}\right] d^2\omega, \tag{4}$$

where the transfer factor between layer n and layer j is defined as

$$\mathcal{F}_{n,j} = \frac{1}{\Delta t_{s,n}} \int_{t_s} \int_0^{2\pi} d\phi \int_\theta \left[e^{t_s - t_{s,j}} - e^{t_s - t_{s,j+1}}\right] \frac{\sin\theta d\theta}{4\pi} dt_s. \tag{5}$$

Let $u = 1/\cos\theta$, then $du = \sin\theta/\cos^2\theta d\theta$ and $\sin\theta d\theta = du/u^2$. Note that the transfer factors given above can be written in terms of the normal optical depth $t = \int_0^z \hat{\kappa_e}(z')dz'$,

$$\begin{aligned}\mathcal{F}_{n,j} &= \frac{1}{2\Delta t_n} \int_t \int_1^\infty \left[e^{(t-t_j)u} - e^{(t-t_{s,j+1})u}\right] \frac{du}{u^2} = \frac{1}{2\Delta t_n} \int_{t_n}^{t_{n+1}} [E_2(t_j - t) - E_2(t_{j+1} - t)]dt \\ &= \frac{1}{2\Delta t_n} [E_3(|t_j - t_{n+1}|) + E_3(|t_{j+1} - t_n|) - E_3(|t_j - t_n|) - E_3(|t_{j+1} - t_{n+1}|)],\end{aligned} \tag{6}$$

where $E_2(\cdot)$ and $E_3(\cdot)$ correspond to the second and third exponential integral functions defined by $E_n(t) = \int_1^{+\infty} \exp(-ut)/u^n du$, which integrate the flux over all solid angles.

The transfer factor $\mathcal{F}_{n,n}$ for a layer to itself (due to emission and scattering) is,

$$\mathcal{F}_{n,n} = 1 - \frac{1}{2\Delta t_n} \int_{t_n}^{t_{n+1}} [E_2(t_n - t) - E_2(t_{n+1} - t)]dt = 1 - \frac{1 - 2E_3(|t_{n+1} - t_n|)}{2(t_{n+1} - t_n)}. \tag{7}$$

For each layer n, the radiosity J_n and irradiance G_n are then,

$$G_n = \sum_{j=0}^{N+1} \mathcal{F}_{n,j} J_j, \qquad J_n = (1 - \tilde{\rho}_n)\,\pi\bar{I}_{b,n} + \tilde{\rho}_n G_n. \tag{8}$$

Note that the ground layer (layer 0) and outer space layer (layer N+1) are included in the calculation because they contribute to the radiative energy balance. The optical depth of two boundaries are set to infinity, i.e. $t_0 = -\infty$ and $t_{N+2} = +\infty$. The G_n and J_n are assembled in a matrix and solved by matrix reduction [8].

2.3 A plating algorithm for plane parallel geometries leads to modified transfer factors

The irradiation on each layer is a result of contributions of all layers. To examine the spectral and vertical contribution to the irradiation on a particular layer n, a modified transfer factor $\mathcal{F}^*_{n,j}$ is defined to express monochromatic irradiation of layer n as,

$$G_n = \sum_{j=0}^{N+1} \mathcal{F}^*_{n,j} \pi\bar{I}_{b,j}. \tag{9}$$

The modified transfer factors $\mathcal{F}^*_{n,j}$ are calculated from the transfer factors $\mathcal{F}_{n,j}$ recursively using a plating algorithm [2]. Note that in Ref. [2], the plating algorithm was used for enclosures with grey surfaces but here the concept of recursive plating is adapted for scattering in and by volumetric atmospheric layers.

The plating algorithm for scattering is initiated by assuming all layers to be non-scattering, i.e., having albedo $\hat{\tilde{\rho}} = 0$,

$$G_n = \sum_{j=0}^{N+1} \mathcal{F}_{n,j} \pi \bar{I}_{b,j}. \tag{10}$$

Then the algorithm applies a single scattering albedo $\hat{\tilde{\rho}}$ value to one layer at a time recursively, starting from layer 0. Non-scattering layers are skipped. Upon the plating of layer k, the radiosity is converted from $\pi \bar{I}_{b,k}$ to J_k, the sum of the emitted and scattered radiation,

$$J_k = (1 - \hat{\tilde{\rho}}_n) \pi \bar{I}_{b,k} + \hat{\tilde{\rho}}_n G_k^*, \qquad \text{and} \qquad G_k^* = \sum_{j \neq k} \mathcal{F}_{k,j} \pi \bar{I}_{b,j} + \mathcal{F}_{k,k} J_k, \tag{11}$$

where * denotes the corrected irradiance value after plating.

Combining the relations in (11) gives the radiosity,

$$J_k = \frac{1 - \hat{\tilde{\rho}}_k}{D_k} \pi \bar{I}_{b,k} + \frac{\hat{\tilde{\rho}}_k}{D_k} \sum_{j \neq k} \mathcal{F}_{k,j} \pi \bar{I}_{b,j}, \tag{12}$$

where the denominator is $D_k = 1 - \hat{\tilde{\rho}}_k \mathcal{F}_{k,k}$.

When i is different from k, the new value of irradiance after plating layer k is given by

$$G_i^* = \sum_{j \neq k} \mathcal{F}_{i,j} \pi \bar{I}_{b,j} + \mathcal{F}_{i,k} J_k = \sum_{j \neq k} \left[\mathcal{F}_{i,j} + \frac{\hat{\tilde{\rho}}_k}{D_k} \mathcal{F}_{i,k} \mathcal{F}_{k,j} \right] \pi \bar{I}_{b,j} + \frac{1 - \hat{\tilde{\rho}}_k}{D_k} \mathcal{F}_{i,k} \pi \bar{I}_{b,k}. \tag{13}$$

The irradiance of layer k itself is then affected by the single scattering albedo,

$$G_k^* = (1 - \hat{\tilde{\rho}}_k) \sum_{j \neq k} \mathcal{F}_{k,j} \pi \bar{I}_{b,j} + (1 - \tilde{\rho}_{s,k}) \mathcal{F}_{k,k} J_k = (1 - \hat{\tilde{\rho}}_k) \sum_{j \neq k} \left[\mathcal{F}_{k,j} + \frac{\hat{\tilde{\rho}}_k}{D_k} \mathcal{F}_{k,k} \mathcal{F}_{k,j} \right] \pi \bar{I}_{b,j} + \frac{(1 - \hat{\tilde{\rho}}_k)^2}{D_k} \mathcal{F}_{k,k} \pi \bar{I}_{b,k}. \tag{14}$$

Compare Eqs.(13) and (14) with Eq. (9) shows that four cases exist,

$$\begin{cases} \mathcal{F}_{i,j}^* = \mathcal{F}_{i,j} + \frac{\hat{\tilde{\rho}}_k}{D_k} \mathcal{F}_{i,k} \mathcal{F}_{k,j}, & i \neq k, j \neq k, \\ \mathcal{F}_{i,k}^* = \frac{1 - \hat{\tilde{\rho}}_k}{D_k} \mathcal{F}_{i,k}, & i \neq k, j = k, \\ \mathcal{F}_{k,j}^* = (1 - \hat{\tilde{\rho}}_k) \left[\mathcal{F}_{k,j} + \frac{\hat{\tilde{\rho}}_k}{D_k} \mathcal{F}_{k,k} \mathcal{F}_{k,j} \right] = \frac{1 - \hat{\tilde{\rho}}_k}{D_k} \mathcal{F}_{k,j}, & i = k, j \neq k, \\ \mathcal{F}_{k,k}^* = \frac{(1 - \hat{\tilde{\rho}}_k)^2}{D} \mathcal{F}_{k,k}, & i = k, j = k. \end{cases} \tag{15}$$

After plating, the modified transfer factors satisfy $\sum_{j=0}^{N+1} \mathcal{F}_{k,j}^* = 1 - \hat{\tilde{\rho}}_k$.

Once the corrected transfer factors are obtained, the energy transfer between each layer can be explicitly calculated using Eq. (9).

3. RESULTS AND DISCUSSION

3.1 Broadband contribution of atmospheric CO_2

Broadband surface downwelling and top of atmosphere (TOA) upwelling longwave radiation as a function of surface water vapor partial pressure and surface CO_2 volumetric mixing ratio w_{CO_2} are plotted in Fig. 2. The surface downwelling flux increases with surface water vapor pressure as well as surface w_{CO_2}, indicating

that water vapor and CO_2 are warming the surface by increasing the downwelling flux. Clearly, CO_2 warming effects are weaker for increased water vapor content because of band overlapping. The CO_2 contribution to surface downwelling flux is around $0.3 \sim 1.2$ W m^{-2} per 100 ppm CO_2 increment, where 1.2 W m^{-2} for drier conditions, and 0.3 W m^{-2} for wetter conditions. The TOA upwelling flux decreases with surface water vapor pressure as well as surface w_{CO_2}, indicating that water vapor and CO_2 are warming the atmosphere by preventing longwave radiation to escape to outer space. Around $0.5 \sim 0.7$ W m^{-2} TOA upwelling longwave flux is decreased per 100 ppm CO_2 increment, where 0.7 W m^{-2} for drier conditions, and 0.5 W m^{-2} for wetter conditions. Note that the calculated effects of CO_2 and H_2O discussed here are first-order effects, without consideration of feedback effects. If feedback is positive, these are lower estimates for the fluxes, if the feedback is negative, then these are upper limit estimates.

3.2 Vertical and spectral contribution to irradiation

Figure 3 presents the vertical and spectral contribution from all layers to the irradiation on a particular layer. The left column and right column show contributions of the modified transfer factor $\mathcal{F}^*_{n,j}$ and monochromatic flux density $\mathcal{F}^*_{n,j}\pi\bar{I}_{b,j}$, respectively.

As shown in Fig. 3 (a1), the transfer factors for the absorbing bands of $0 \sim 400$ cm^{-1} (H_2O), $650 \sim 750$ cm^{-1} (CO_2), $1400 \sim 1700$ cm^{-1} (H_2O) and $2300 \sim 2400$ cm^{-1} (CO_2) are near unity, indicating the surface downwelling flux in these bands are mostly coming from the nearest atmosphere layer (Fig.3 (a2)). Comparing Fig. 3 (a1) and (a2), the latter two bands show relatively smaller contributions in (a2) than in (a1) because $\bar{I}_b$ is relatively small in these two bands.

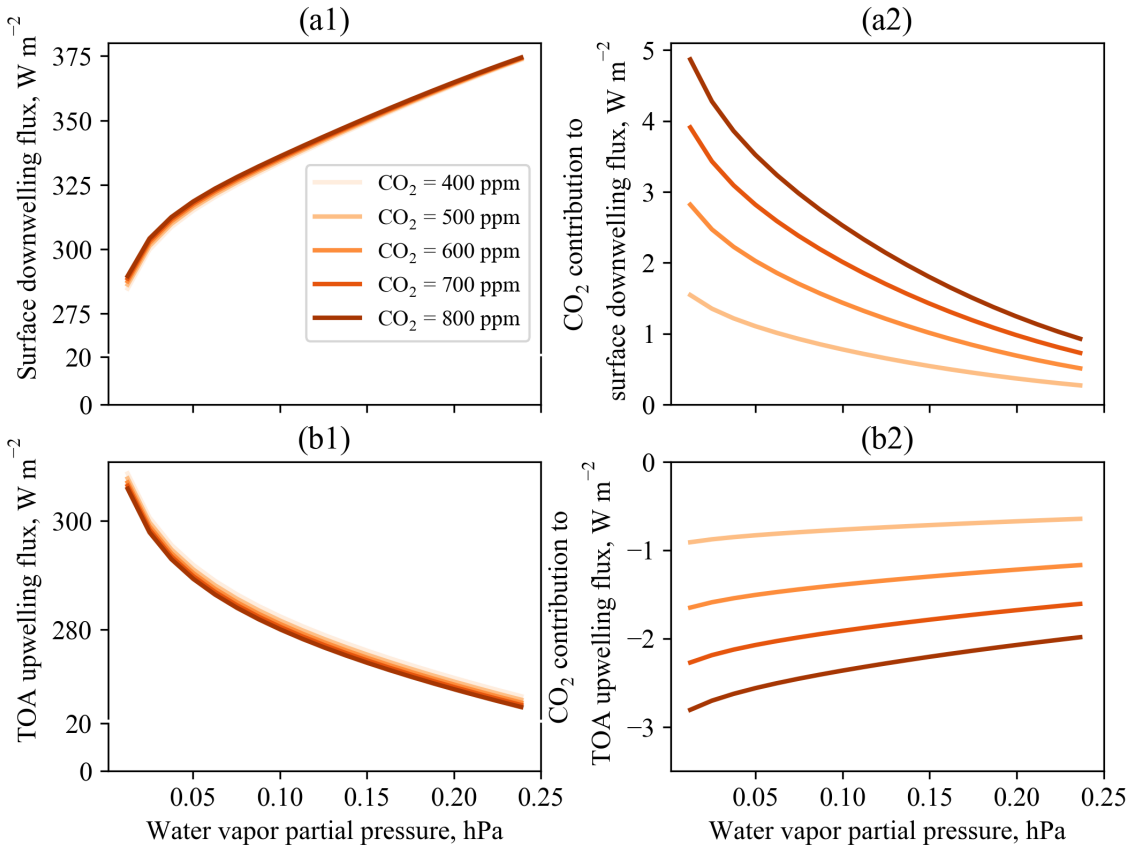

Fig. 2 Broadband contribution of atmospheric CO_2 to (a) surface downwelling and (b) TOA upwelling fluxes.

Fig. 3 (b1) shows that the transfer factors to the nearest atmosphere layer are near unity in the four absorbing bands from the layer itself. The transfer factor from the ground layer is around 0.5 in the atmospheric window bands, i.e. 400 $\sim$ 650 cm^{-1}, 750 $\sim$ 1400 cm^{-1}, 1700 $\sim$ 2300 cm^{-1} and 2400 $\sim$ 2500 cm^{-1}. Fig. 3 (b2) shows the contributions to flux density from bands larger than 2000 cm^{-1} are negligible because of small $\bar{I}_b$.

Fig. 3 (c1) shows that the transfer factor from the tropo-pause layer to itself in the four absorbing bands is the largest compared with from other layers. Notably, the absorbing bands of CO_2 are near unity while the absorbing bands of water vapor are around 0.6 because little water vapor is presented at that altitude (10.48 km $\sim$ 12.60 km) but CO_2 is well mixed below 40 km. The transfer factor from the outer space is around 0.5 except the absorbing bands of CO_2. The contribution to flux density from the outer space is negligible as shown in Fig. 3 (c2), because there is only 1% longwave in extraterrestrial solar radiation. The ground layer contributes partially to the transfer factor and the flux density in the window bands.

Fig. 3 (d1) shows that the transfer factor from the outer space to the top atmosphere layer dominates. Other contributions come from the ground layer in the window bands, from the middle of atmosphere in the water vapor absorbing bands and from the top of atmosphere in the CO_2 absorbing bands. For flux density in Fig. 3 (d2), contributions from the outer space vanishes, leave only contributions from the surface and the middle atmosphere in bands smaller than 1200 cm^{-1}.

Fig. 3 (e1) shows that the transfer factor from the surface to the outer space in the window bands is the largest. Other contributions come from the water vapor absorbing bands in the middle of atmosphere and CO_2 absorbing bands in the top of atmosphere. For flux density in Fig. 3 (e2), contributions from bands larger than 1200 cm^{-1} vanish.

3.3 Broadband contribution to irradiation from each layer

For an atmosphere with surface relative humidity of 65% and aerosol optical depth at 479.5 nm equal to 0.1, the broadband percentage contributions of the transfer factor and irradiation flux of each layer are illustrated in Fig. 4 (a) and (b), respectively. The summation of each row in Fig. 4 equals to 100%. The outer space layer (layer 19) dominants the transfer factor to upper layers (above tropopause) but the flux contribution is negligible. For the surface layer, 64.4% of its longwave irradiation comes from the nearest atmospheric layer, 15.3% comes from the 2nd nearest layer, 7.5% comes from the 3rd nearest layer and the remainder 12.8% comes from all other layers. For the nearest atmosphere layer, 27.4% of its longwave irradiation comes from the surface, 52.5% comes from itself, 11.2% comes from the layer above it and the rest 8.9% comes from all other layers. Similarly, 18.0% of the 2nd nearest atmospheric layer longwave irradiation comes from the surface, 4.3% comes from the layer below it, 63.2% comes from itself, 8.1% comes from the layer above it, while the remainder 6.4% comes from other layers. From the nearest atmosphere layer to the tropopause layer (layer 13), the largest contribution to the irradiation on the layer is from the layer itself. Above the tropopause, the largest contribution is from the ground layer. The layers above the tropopause contribute less than 4.8% to the irradiance to other layers due to lower temperature levels.

4. CONCLUSIONS

Here we discuss the longwave radiative process in different layers of the Earth's atmosphere, and present a method to quantify the spectral and vertical contributions of longwave radiation for each layer. The atmosphere model is a partially scattering medium with aerosols, so each atmosphere layer is treated analogously to a *gray surface* in a radiative enclosure problem where transfer factors are evaluated between surfaces and surfaces, between volumes and volumes, and between surfaces and volumes. A radiosity-irradiation balance for each layer is applied to solve for the irradiation and radiosity fluxes for all layers. Then the irradiation of each layer is decomposed as the summation of weighted blackbody emission from all other layers. The weights are the modified transfer factors, which are found by application of a recursive plating algorithm to the each layer.

Numerical results are presented for an atmosphere with surface relative humidity of 65% and aerosol optical depth at 479.5 nm equal to 0.1. First order broadband contributions of increased atmospheric CO_2 to surface downwelling flux is found to be 0.3 $\sim$ 1.2 W m^{-2} per 100 ppm CO_2 increment for different water vapor contents. The broadband reduction of TOA upwelling flux is found to be 0.5 $\sim$ 0.7 W m^{-2} per 100 ppm CO_2 increment. The contribution to surface downwelling fluxes in the four absorbing bands comes mostly from the nearest layers. The contribution to the irradiation on the nearest layer within the four absorbing bands comes mostly from the layer itself. The ground layer contributes substantially to the irradiance in the window bands. The irradiation on the tropopause layer in the four absorbing bands mostly comes from itself, and the two absorbing bands of CO_2 have noticeably larger contribution than the two water vapor bands, because little water vapor is present at the tropopause altitude while CO_2 is well mixed below 40 km. The surface

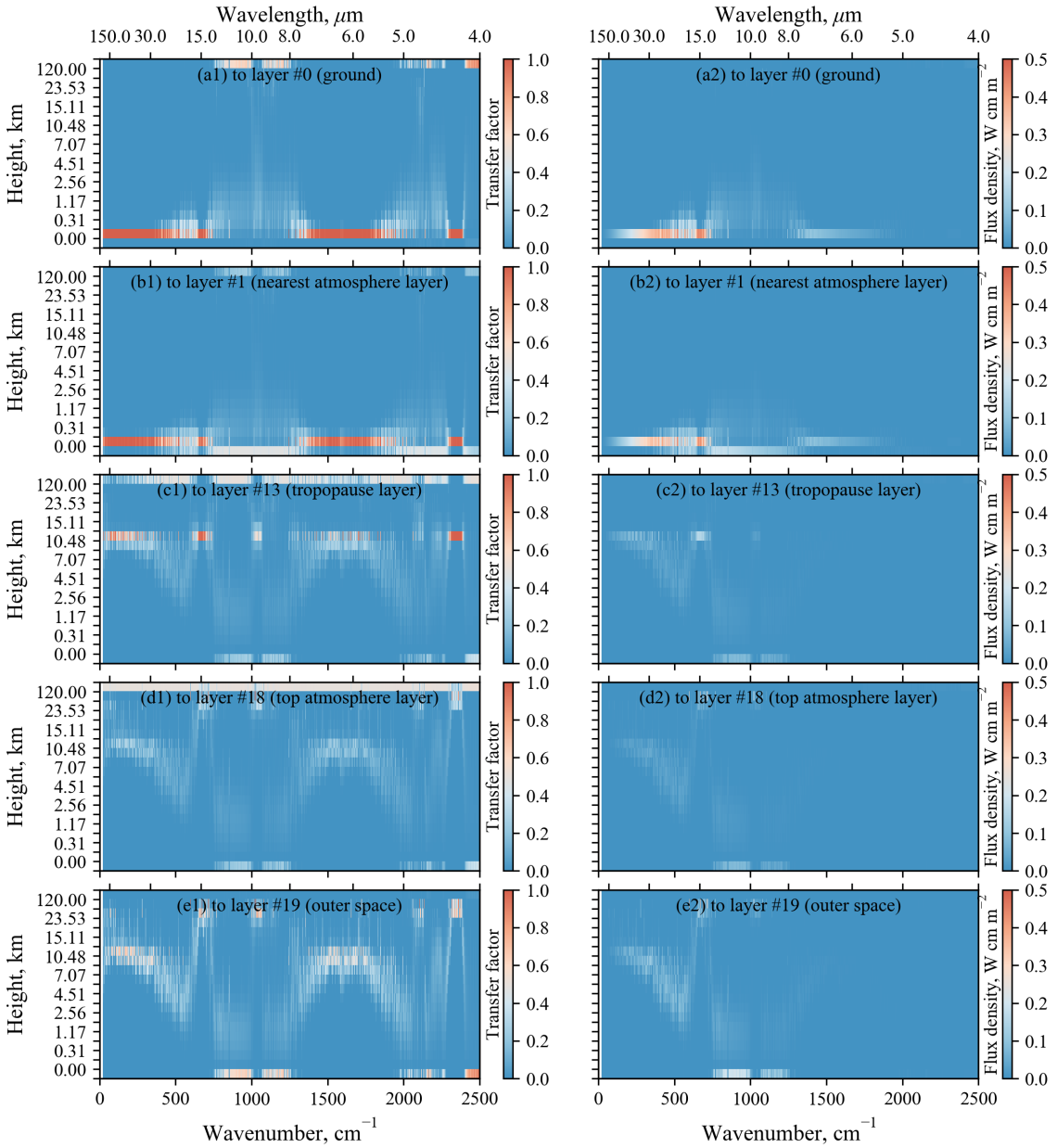

Fig. 3 Vertical and spectral contribution of irradiation on selected layers: (a) ground layer, (b) nearest atmosphere layer, (c) tropopause layer, (d) top atmosphere layer and (e) outer space layer. Surface RH = 65% and $AOD_{497.5}$ = 0.1.

also contributes to a large portion in the atmospheric window bands. Contributions to the irradiation on the top atmosphere layer and outer space layer come from the surface in the atmospheric window bands, from the middle of atmosphere in the water vapor absorbing bands and from the top of atmosphere in the CO_2 absorbing bands. For broadband flux contributions, the outer space layer dominates the transfer factors to upper layers (above the tropopause) but the flux contribution is negligible due to low densities and effective temperatures at that level. For the ground layer, 64.4%, 15.3% and 7.5% of its longwave irradiation comes from the nearest atmospheric layer, the 2nd nearest layer and the 3rd nearest layer, respectively. For all layers below the tropopause, the layer itself contributes the most to its irradiation. For layers above the tropopause layer, the largest contributor to its irradiation is the ground layer. Finally, upper layers above the tropopause contribute to less than 4.8% to the irradiance flux to other layers.

In summary, the efficient model proposed in this work allows for rapid calculation of the spectral and vertical distributions of atmospheric longwave radiation under clear sky conditions, and can be readily deployed for different temperature profiles, gas or aerosol concentrations.

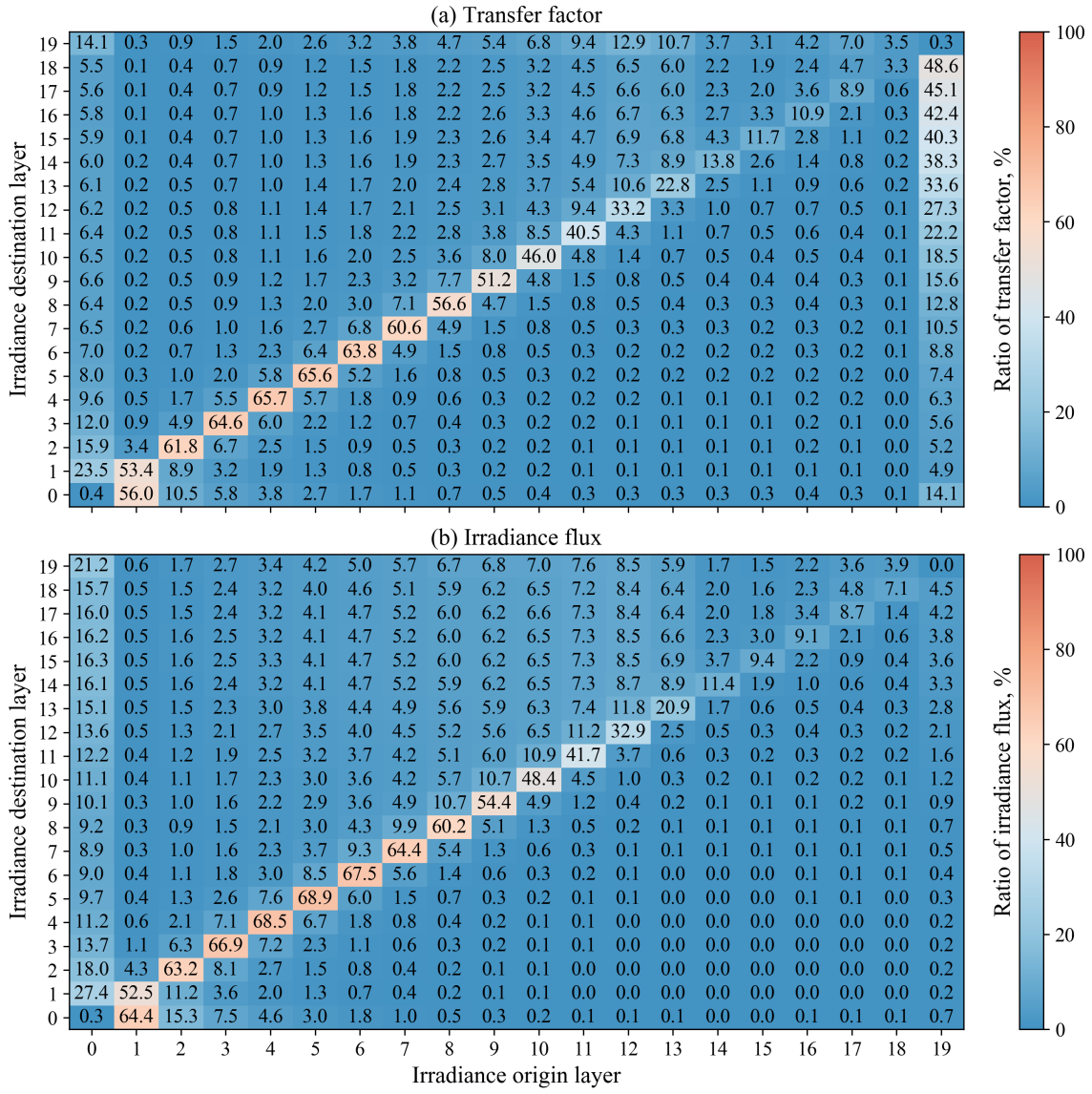

Fig. 4 The broadband percentage contributions of the transfer factor (a) and irradiance flux (b) of each layer. Surface RH = 65% and $AOD_{497.5}$ = 0.1. The total contributions in each row add to 100 (%).

REFERENCES

[1] Anderson, G. P., Clough, S. A., Kneizys, F. X., Chetwynd, J. H., and Shettle, E. P., "AFGL atmospheric constituent profiles (0.120 km)," , Tech. rep., Air Force DTIC Document, (1986).

[2] Edwards, D. K., "The plating algorithm for radiation script-F transfer factor," *ASME Journal of Heat Transfer*, 108(1), pp. 237–238, (1986).

[3] Gordon, I. E., Rothman, L. S., Hill, C., Kochanov, R. V., Tan, Y., Bernath, P. F., Birk, M., Boudon, V., Campargue, A., Chance, K., , "The HITRAN2016 molecular spectroscopic database," *Journal of Quantitative Spectroscopy and Radiative Transfer*, 203, pp. 3–69, (2017).

[4] Huang, Z. and Ruan, X., "Nanoparticle embedded double-layer coating for daytime radiative cooling," *International Journal of Heat and Mass Transfer*, 104, pp. 890–896, (2017).

[5] Landro, B. and McCormick, P., "Effect of surface characteristics and atmospheric conditions on radiative heat loss to a clear sky," *International Journal of Heat and Mass Transfer*, 23(5), pp. 613–620, (1980).

[6] Lee, M., "Scaling anisotropic scattering in radiation heat transfer for a planar medium," *Urbana*, 2, pp. 61801, (1982).

[7] Li, M., Jiang, Y., and Coimbra, C. F. M., "On the determination of atmospheric longwave irradiance under all-sky conditions," *Solar Energy*, 144, pp. 40–48, (2017).

[8] Li, M., Liao, Z., and Coimbra, C. F. M., "Spectral model for clear sky atmospheric longwave radiation," *Journal of Quantitative Spectroscopy and Radiative Transfer*, 209, pp. 196–211, (2018).

[9] Mlawer, E. J., Payne, V. H., Moncet, J.-L., Delamere, J. S., Alvarado, M. J., and Tobin, D. C., "Development and recent evaluation of the MT_CKD model of continuum absorption," *Philosophical Transactions of the Royal Society of London A: Mathematical, Physical and Engineering Sciences*, 370, pp. 2520–2556, (2012).

[10] Philipona, R., Dutton, E. G., Stoffel, T., Michalsky, J., Reda, I., Stifter, A., Wendung, P., Wood, N., Clough, S. A., Mlawer, E. J., , "Atmospheric longwave irradiance uncertainty: Pyrgeometers compared to an absolute sky-scanning radiometer, atmospheric emitted radiance interferometer, and radiative transfer model calculations," *Journal of Geophysical Research: Atmospheres*, 106(D22), pp. 28129–28141, (2001).

[11] Shimazaki, Y., Yoshida, A., and Yamamoto, T., "Investigation of heat transfer and temperature distribution in outdoor human–clothing–environment systems with double-layered ensemble," *International Journal of Heat and Mass Transfer*, 115, pp. 523–529, (2017).

[12] Zhou, X., Xu, Y., and Zhang, F., "Evaluation of effect of diurnal ambient temperature range on solar chimney power plant performance," *International Journal of Heat and Mass Transfer*, 115, pp. 398–405, (2017).